COMPARISON OF OXYGEN CARRIERS FOR CHEMICAL-LOOPING COMBUSTION

by

Marcus JOHANSSON, Tobias MATTISSON, and Anders LYNGFELT

Original scientific paper
UDC: 662.612/.613-977
BIBILID: 0354-9836, *10* (2006), 3, 93-107

Chemical-looping combustion is a combustion technology with inherent separation of the greenhouse gas CO_2. This technique involves combustion of fossil fuels by means of an oxygen carrier which transfers oxygen from the air to the fuel. In this manner a decrease in efficiency is avoided for the energy demanding separation of CO_2 from the rest of the flue gases. Results from fifty oxygen carriers based on iron-, manganese- and nickel oxides on different inert materials are compared. The particles were prepared using freeze granulation, sintered at different temperatures and sieved to a size 125-180 μm. To simulate the environment the particles would be exposed to in a chemical-looping combustor, reactivity tests under alternating oxidizing and reducing conditions were performed in a laboratory fluidized bed-reactor of quartz. Reduction was performed in 50% CH_4/50% H_2O while the oxidation was carried out in 5% O_2 in nitrogen. In general nickel particles are the most reactive, followed by manganese. Iron particles are harder but have a lower reactivity. An increase in sintering temperatures normally leads to an increase in strength and decrease in reactivity. Several particles investigated display a combination of high reactivity and strength as well as good fluidization behavior, and are feasible for use as oxygen carriers in chemical-looping combustion.

Key words: *chemical-looping combustion, CO_2 capture, oxygen-carriers, iron oxide, manganese oxide, nickel oxide*

Introduction

Chemical-looping combustion

Chemical-looping combustion (CLC) is a combustion technology where an oxygen carrier is used to transfer oxygen from the combustion air to the fuel, thus avoiding direct contact between air and fuel [1-3]. The process is composed of two fluidized reactors, an air and a fuel reactor, as shown in fig. 1. The fuel is introduced to the fuel reactor in a gaseous form where it reacts with an oxygen carrier to CO_2 and H_2O. The reduced oxygen carrier is transported to the air reactor where it is oxidized back to its original state by air. The fuel could be syngas from coal gasification, natural gas, or refinery gas. The overall reactions in the reactors are:

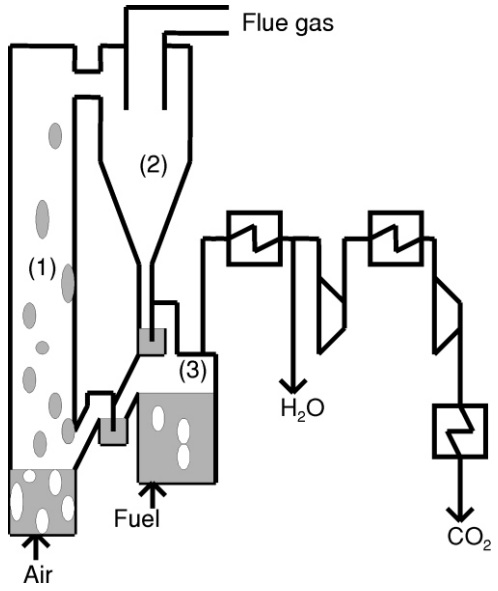

Figure 1. Schematic view of chemical-looping combustion
(1) Air reactor and riser
(2) Cyclone
(3) Fuel reactor

Fuel reactor: $(2n + m)M_yO_x + C_nH_{2m} \quad (2n + m)M_yO_{x\ 1} + mH_2O + nCO_2$ (1)

Air reactor: $(2n + m)M_yO_{x\ 1} + (n + ½m)O_2 \quad (2n + m)M_yO_x$ (2)

Net reaction: $C_nH_{2m} + (n + ½m)O_2 \quad mH_2O + nCO_2$

Reaction (1) is either endothermic or exothermic, depending on type of fuel and oxygen carrier, while reaction (2) is always exothermic. The total amount of heat evolved from reaction (1) plus (2) is the same as for normal combustion where the oxygen is in direct contact with the fuel. However, the advantage with this system compared to normal combustion is that the CO_2 and H_2O are inherently separated from the rest of the flue gases, and no major energy is expended for this separation. Thus, compared to other technologies for capture of CO_2, CLC is potentially much cheaper since no costly gas-separation equipment is necessary [4]. Although a real process could be either pressurized or atmospheric, a first step is to investigate CLC under atmospheric conditions. Expected temperature range could be at least 800-1200 ºC for the fuel- and air-reactor, although the temperature would be higher in the air reactor for the cases when reaction (1) is endothermic. A CLC system of fluidized bed reactors adapts technology and components proven in applications such as circulating fluidized-bed combustion [3]. The key issue for the process is to find an oxygen carrier which is:

– reactive towards the fuel gas and air,
– resistant towards attrition,
– not apt to agglomerate, and
– possible to produce at reasonable cost.

Oxygen carriers

In a thermodynamic analysis of different oxygen carriers, Mattisson and Lyngfelt found that some metal oxides of the transition state metals Fe, Mn, and Ni were among the feasible candidates to be used as oxygen carriers in CLC run at higher temperatures [5]. These metal oxides are preferably supported by an inert material which is believed to increase the reactivity and help to maintain the internal structure of the particles throughout the redox reactions. For other comparisons of oxygen carriers for chemical-looping combustion, and relevant references, see work by Mattisson and co-workers [3, 6, 7] and Adánez *et al*. [8]. In the present work oxygen carriers based on the metal oxides Fe_2O_3, NiO, and Mn_3O_4 were prepared with different inert materials. The selection of the inert materials was chosen from previous work, both within CLC and heterogeneous catalysis, where such material has been found to be suitable as carrier material for transition state metals and metal oxides.

Experimental

Preparation of oxygen carriers

All the particles were produced by freeze-granulation in the following manner. A water-based slurry of the composite material, in the form of chemical powders with a size less than 10 m, and a small amount of polyacrylic acid as dispersant were prepared by ball milling for 24 h. After milling, some polyvinyl alcohol was added to the slurry as a binder to keep the particles intact during later stages in the production process, *i. e.* freeze-drying and sintering. Spherical particles were produced by freeze-granulation, *i. e*. the slurry is pumped to a spray nozzle where passing atomising-air produce drops, which are sprayed into liquid nitrogen where they freeze instantaneously. The frozen water in the resulting particles is then removed by sublimation in a freeze-drier operating at a pressure that corresponds to the vapour pressure over ice at 10 ºC. After drying, the particles were sintered at temperatures between 950 and 1600 ºC for 6 h using a heating rate of 5 ºC/min. Finally they were sieved to obtain particles of well-defined sizes.

In tab. 1 the fifty oxygen carriers investigated in this paper are presented. For these carriers, parameters such as ratio of metal oxide/inert, sintering temperature and type of inert are varied. Notice that two NiO on $NiAl_2O_4$ were investigated. The differences of these, besides the different sintering temperatures used, are that two different types of Al_2O_3 were used as starting material. Particle 34 was prepared using an ultra pure -Al_2O_3 whereas particle 35 was prepared with a technical grade -Al_2O_3. The nomenclature used here for the different oxygen carriers is given in column 2 in tab. 1, and in the text these abbreviations will be followed by the sintering temperature, *i. e*. F4S950 corresponds to 40% Fe_2O_3/60% SiO_2 sintered at 950 °C.

Table 1. Oxygen carriers investigated in this paper

Oxygen carrier composition	Abbr.	Sintering temperature [°C]									
		950	1100	1125	1150	1175	1200	1300	1400	1500	1600
40% Fe_2O_3/60% SiO_2	F4S	S	S					S			
40% Fe_2O_3/60% ZrO_2	F4Z	1	2					3			
60% Fe_2O_3/32% Al_2O_3 + 8% Bentonite	F6AB		4				5	6			
40% Fe_2O_3/60% $MgAl_2O_4$	F4AM		7				8	9			
60% Fe_2O_3/40% $MgAl_2O_4$	F6AM		10	11	12	13	14				
80% Fe_2O_3/20% $MgAl_2O_4$	F8AM		15				16	17			
37% Mn_3O_4/63% SiO_2	M37S	S	18				L	L			
37% Mn_3O_4/63% ZrO_2	M37Z	19	20					21			
40% Mn_3O_4/60% Ca-ZrO_2	M4CZ	22	23				24	25			
40% Mn_3O_4/60% Mg-ZrO_2	M4MZ	26	27		28		29	30			
40% Mn_3O_4/60% Ce-ZrO_2	M4CeZ	31	32					33			
40% NiO/60% $NiAl_2O_4$	N4AN							34			
40% NiO/60% $NiAl_2O_4$	N4AN										35
40% NiO/48% $NiAl_2O_4$ + 12% CaO	N4AC								36		C
40% NiO/48% $NiAl_2O_4$ + 12% Bentonite	N4AB							37			
60% NiO/40% $MgAl_2O_4$	N6AM								38	39	40
60% NiO/40% MgO	N6M		S				S	L			

S – particles being too soft
L – limited or no reactivity
C – sintered to cake at heat treatment
Black fields with number indicate further investigated particles

Characterization of fresh and reacted oxygen carriers

In order to determine possible chemical transformations that occurred in the samples during sintering and reaction, all of the fresh and reacted samples were characterized using X-ray powder diffraction (Siemens D5000 Powder Diffractometer utilizing Cu K radiation). Also the shape and morphology of both fresh and reacted oxygen carrier particles were studied using a light microscope as well as an analytical scanning electron microscope (Electroscan 2020). Because of the need for the oxygen carrier to be resistant towards fragmentation and attrition, the force needed to fracture the particles was measured using a Shimpo FGN-5 crushing strength apparatus. The crushing strength was

measured on particles in the size range 180-250 m and taken as the average value of 30 results.

Reactivity investigation

Methane was chosen as reacting gas for the particle comparison, because it facilitates the experimental procedure. The results can be expected to give a measure for the ranking of particle reactivity, highly relevant also for other fuel gases like CO and H_2. In a subsequent study the best particles are compared using syngas [9]. The experiments were conducted in a laboratory fluidised-bed reactor of quartz. The reactor had a length of 820 mm with a porous quartz plate of 30 mm in diameter placed 370 mm from the bottom. The inner diameters of the bottom and top sections were 19 and 30 mm. The temperature was measured 5 mm under, and 38 mm above the porous quartz plate, using 10% Pt/Rh thermocouples enclosed in quartz shells. A sample of 10 or 15 g of oxygen carrier particles, in the size range of 125-180 m, was initially heated in an inert atmosphere to 950 °C. The metal oxides investigated in this work had a large difference in apparent density (800-4500 kg/m^3), and thus the bed heights also varied in a wide range, between 4-33 mm. Because of the heat produced during the oxidation period, a gas mixture with 5% O_2 in N_2 was used instead of air. Thus, large temperature increases were avoided. The particles were then exposed alternatively to 5% O_2 and 50% CH_4 /50% H_2O, thus simulating the cyclic conditions of a CLC system. To avoid air and methane mixing during the shifts between reduction and oxidation, nitrogen gas was introduced during 180 s after each period. The particles were tested in this manner for 4-17 cycles, depending on the reactivity. The gas from the reactor was led to an electric cooler, where the water was removed, and then to a gas analyser where the concentrations of CO_2, CO, CH_4, and O_2 were measured in addition to the gas flow. The experiments with a 10 g bed were conducted with an inlet gas flow of 600 ml_n/min. for the reducing gas, while for the 15 g bed the gas flow was 900 ml_n/min. Hence the ratio of gas flow/bed mass was held constant which makes the experiments comparable. For the oxidizing gas, the gas flow was either 600 or 1000 ml_n/min. This corresponds to 2-12 u_{mf} and 4-15 u_{mf} for the incoming reducing and oxidizing gases respectively, where u_{mf} is the minimum fluidisation velocity. However, as three moles of product gas are formed for every mole of reacted CH_4, the velocity may be as high as 4-24 u_{mf}.

The evaluation method will be described briefly, and for a more detailed description see other work from Mattisson and co-workers [7, 10, 11]. The degree of oxidation, or conversion, is defined as:

$$X \quad \frac{m \quad m_{red}}{m_{ox} \quad m_{red}} \tag{3}$$

where m is the actual mass of sample, m_{ox} is the mass of the sample when fully oxidized and m_{red} the mass of the sample in the fully reduced form. In order to facilitate a

comparison between different oxygen carriers that contain varying amounts of oxygen depending upon the fraction of inert, a mass-based conversion was defined as:

$$\omega \quad \frac{m}{m_{ox}} \quad 1 \quad R_o(X \quad 1) \tag{4}$$

where R_o is the oxygen ratio, defined as:

$$R_o \quad \frac{(m_{ox} \quad m_{red})}{m_{ox}} \tag{5}$$

The oxygen ratio is the maximum mass fraction of the oxygen-carrier that can be used in the oxygen transfer, and is dependent on the metal oxide used as oxygen carrier as well as the amount of inert in the particles.

To facilitate a comparison of reaction rates between different oxygen carriers a rate index was defined as the normalized rate, expressed in %/min.:

$$\text{Rate index} \quad 60 \ 100 \quad \left(\frac{d\omega}{dt}\right)_{norm} \tag{6}$$

where $\left(\frac{d\omega}{dt}\right)_{norm}$ is the normalized average rate expressed in s^{-1}, and calculated from:

$$\left(\frac{d\omega}{dt}\right)_{norm} \quad k_{eff} p_{ref} \tag{7}$$

where p_{ref} is a reference partial pressure of methane, here equal to 0.15, which would approximately correspond to a full conversion of the gas (see discussion below). If the mass transfer resistance between the bubble and emulsion phases in the fluidized bed reactor is small, and assuming that the reaction between the methane and solid is first order with respect to methane, the exposure of particles to methane can be represented by a log-mean partial pressure of methane, p_m, which can be defined in terms of the inlet and outlet partial pressure:

$$p_m \quad \frac{p_{in} \quad p_{out}}{\ln \frac{p_{in}}{p_{out}}} \tag{8}$$

Assuming an inlet partial pressure of methane of 1 and an outlet partial pressure of 0.001 the log-mean partial pressure would be 0.145, eq. 8. The fact that all of the oxy-

gen was consumed in the initial part of the oxidation period (see fig. 4b and d), suggests that there was good contact between all reacting gas and the particles in the reactor.

The effective first order reaction rate constant, k_{eff} in eq. 7, was calculated from:

$$k_{\text{eff}} \quad \frac{1}{p_{\text{m}}} \frac{\text{d}\omega}{\text{d}t} \tag{9}$$

For calculations of the rate index and the normalized rate of reaction in eq. (6) and (7) the average rate constant in the interval of $\omega = 0.01$ where the reactivity is the fastest was chosen. The choice of interval depends on the endothermic reaction in the fuel reactor, for which the recirculation rate needs to be sufficient to avoid large temperature drops in the fuel reactor. This interval corresponds to a recirculation rate of particles of 8 kg/s MW_t [7] corresponding to a temperature drop in of less than 50 °C.

Results and discussion

Analysis of fresh oxygen carriers

In fig. 2a is shown a light microscopy image of M4MZ1100. Furthermore figs. 2b and 2c show SEM images of the same particle. It can clearly be seen that the particles are spherical and that that they display a smooth granular structure. Most particles investigated in this study have a similar appearance as the one shown in fig. 2.

As seen in tab. 1 some of the prepared oxygen carriers were too soft and did not become spherical granulates after the sintering process. These are represented with an "S" in tab. 1, and are all three samples of Fe_2O_3/SiO_2, Mn_3O_4/SiO_2 sintered at 950 °C and NiO/MgO sintered at 1100 and 1200 °C. For NiO/CaO-$NiAl_2O_4$ sintered at 1600 °C, a single hard agglomerate was formed. For obvious reasons these mentioned particles were

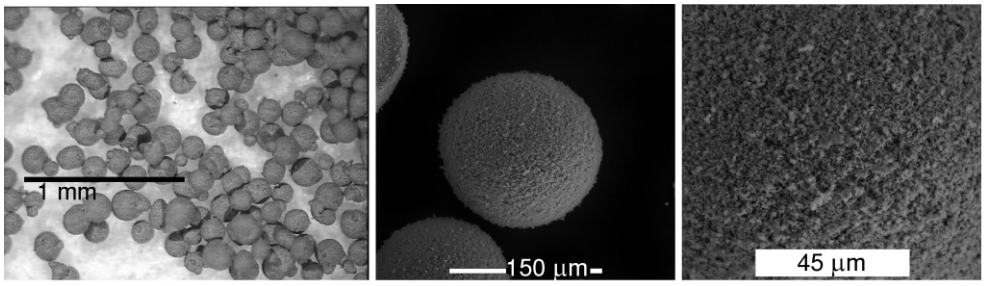

Figure 2. Freeze granulated particles of M4MZ1100
(a) Light microscope image (black bar = 1 mm), (b) SEM image of particle (horizontal bar at bottom = 150 µm), and (c) SEM image of surface (horizontal bar at bottom = 45 µm)

unsuitable for further testing for chemical-looping combustion. For almost all particles an increase in strength is observed when the sintering temperature is increased. This can be seen for the iron based carriers in fig. 3. The same trend has also previously been shown for manganese based oxygen carriers [12].

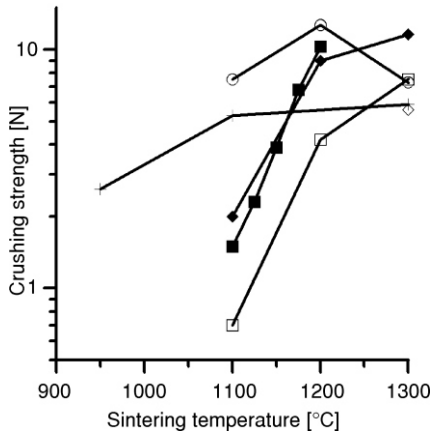

Figure 3. Crushing strength as a function of the sintering temperature for iron particles

F4Z
F6AB
F4AM
F6AM, and
F8AM

Analysis of reacted oxygen carriers

Figures 4a-d shows the outlet concentration of gaseous components for one reduction and one oxidation period conducted with an iron- and a nickel particle. During the reduction in figs. 4a and 4c, the incoming methane initially reacts completely to form mainly CO_2 and H_2O for both particles. For nickel oxides there is however a thermodynamic limitation [5], and hence some CO and H_2 are at all times present during the reduction. As the reaction proceeds and the degree of conversion is lower, the two particles behave differently. For iron, a large proportion of the methane pass unreacted through the bed and there is formation of some minor amounts of CO and H_2. H_2 is not measured on-line, but is assumed to be related to the outlet partial pressure of CO and CO_2 through an empirical relation based on the equilibrium of the water-shift reaction. Since it was not measured on-line, it is not presented in the figures. For nickel, CH_4 does not pass through the reactor unreacted, but reacts to CO and H_2, most likely through methane pyrolysis or steam reforming. Formation of carbon can also be detected for some nickel oxides when the reduction is allowed to proceed for a long time, *i. e*. when there is only a small amount of NiO left in the particles. This was detected by CO and/or CO_2 from the outlet of the reactor during both the inert and oxidizing periods. As for the oxidations in figs. 4b and 4d, full conversion of the incoming oxygen occurs initially. This means that the oxidation is fast and also limited by the supply of oxygen in these experiments. The major focus will

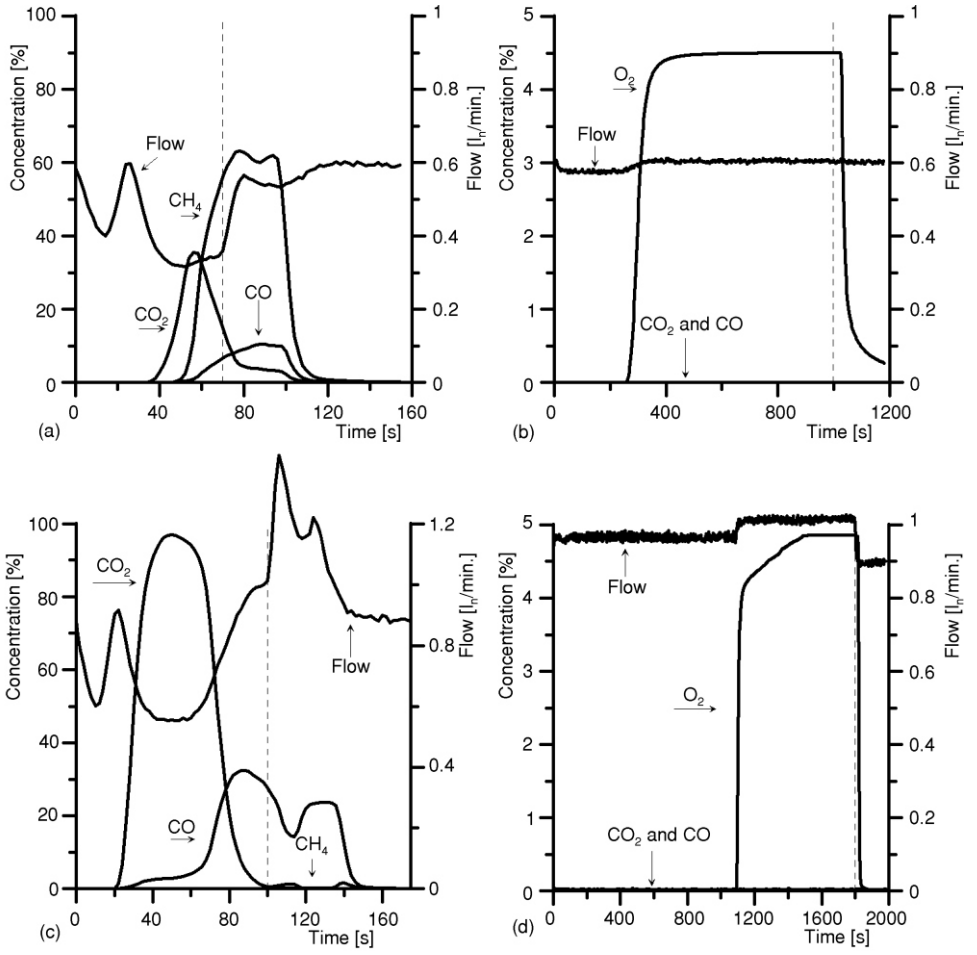

Figure 4. Concentration profiles of reduction (a) and oxidation (b) of F4AM950, and reduction (c) and oxidation (d) of N6AM1400; vertical dashed lines indicate transition to inert gas

therefore be on the reduction of the particles in this paper. The concentration profiles in figs. 4a-d are typical for iron and nickel oxides. For manganese based oxygen carriers the profiles are similar to iron, although in general somewhat more reactive.

As indicated in tab. 1, three oxygen carriers did not show any significant reactivity at all, these were M37S1200, M37S1300, and N6M1300. The reason for this is most likely associated with the formation of irreversible compounds through solid state reactions that occurred between metal oxide and inert material during heat treatment (see below). For this reason these three particles are not considered to be suitable for chemical-looping combustion.

In figs. 5a-c the rate index *vs*. crushing strength is shown for iron, manganese, and nickel based oxygen carriers. Note that the scales are logarithmic and differs significantly between the three figures. Also included in the figures are the particles which de-fluidized at some point during reaction, represented by circles. De-fluidization here means that a small force was necessary to separate the particle from each other after an experiment. The phenomenon of de-fluidization of oxygen carriers is not easy to define or understand, it was however clear that no severe agglomeration occurred at any of the investigated particles. Furthermore, experiments on the same particles in other reactors indicate that the problem of de-fluidization can be avoided by using larger height/width ratio of the bed, or by simply avoiding the reduction of the particles to too low degrees of conversion. Cho *et al*. found that iron oxide particles on alumina de-fluidized only when there was significant FeO formation [11]. Thus, de-fluidization may not necessarily have

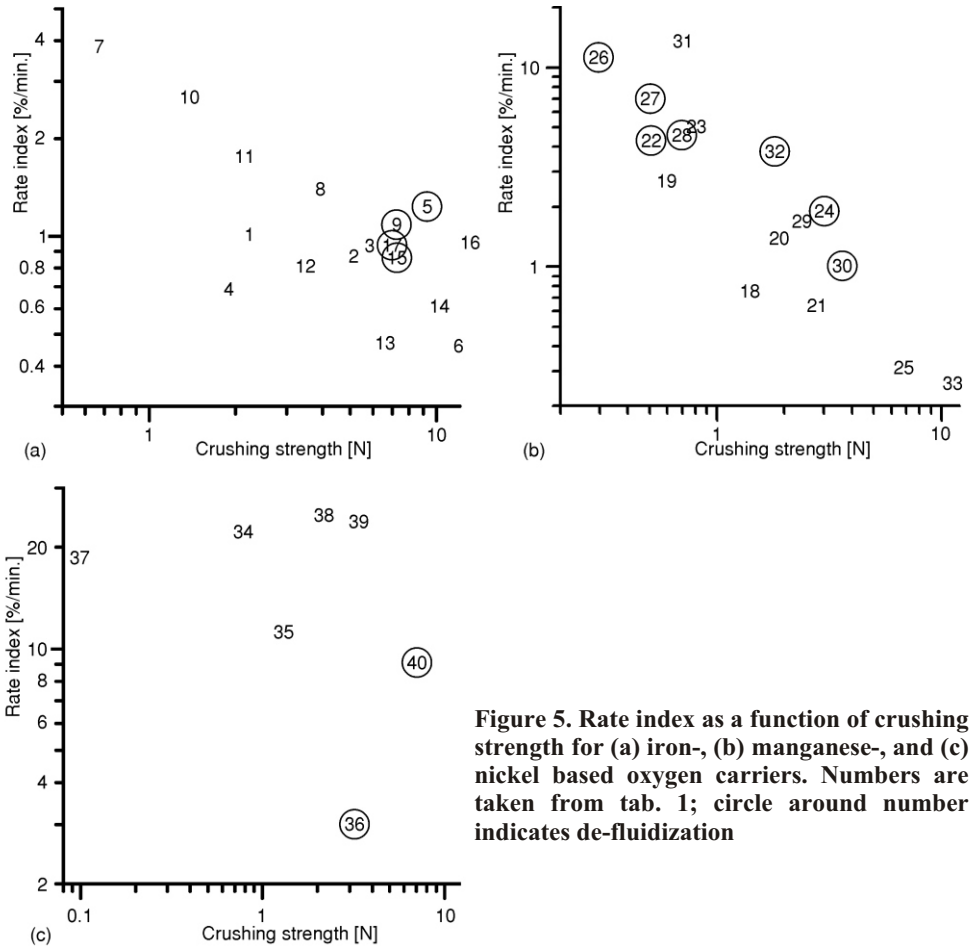

Figure 5. Rate index as a function of crushing strength for (a) iron-, (b) manganese-, and (c) nickel based oxygen carriers. Numbers are taken from tab. 1; circle around number indicates de-fluidization

to be a problem at scale-up. The tendency that hard particles are less reactive is clearly seen for the iron- and manganese particles. Since hard particles normally are less porous, it is not surprising that their reactivity is lower.

For iron, F4AM1100 and F6AM1100 (#7 and #10), seem to best suited for chemical-looping combustion, if the properties of reactivity, strength and good fluidization-behavior are all taken into consideration. These particles have already been investigated by Johansson *et al*. [10]. Based on the same criteria, M4CeZ950 and M4CZ1100 (#31 and #23) would be the best option for the manganese oxides. However, more particles could be considered as suitable if de-fluidization is not a problem in a real application. For instance, M4MZ1150 (#28) has successfully been used as an oxygen carrier in a continuously working CLC reactor for 70 hours without de-fluidization [13]. For nickel, N6AM1400 and N6AM1500 (#38 and #39) are the most promising particles; although both N4AN particles (#34 and #35) showed relatively high strength and reactivity. N4AB1300 (#37) is also very reactive but may be too soft to be suitable in a real application.

When comparing all oxygen carriers it becomes clear that the nickel oxides are by far the most reactive ones. This can be seen in fig. 6. where all investigated particles are displayed in one graph as rate index *vs*. crushing strength. Furthermore, the reactivities of the most reactive nickel oxides are limited by the supply of incoming methane in the experiments, as can be seen in fig. 4c. This means that the rate indexes presented for some nickel oxides are underestimated. The iron oxides are in general the hardest but not very reactive, whereas the manganese based carriers seem to be somewhere in-between nickel and iron in strength and reactivity. In general, de-fluidization mainly seems to concern manganese based oxygen carriers.

In tab. 2 are found results from the X-ray powder diffraction (XRD) of fresh particles and used particles removed from the reactor after the last reduction period. As mentioned above, for the particles that had a very little or no reactivity, (M37S1200,

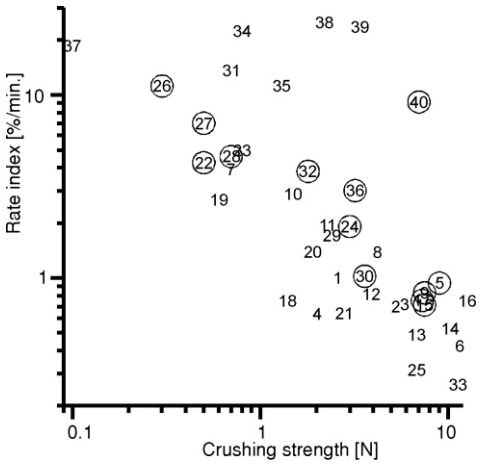

Figure 6. Rate index as a function of crushing strength for all the investigated particles. Numbers are taken from tab. 1; circle around number indicates de-fluidization

Table 2. XRD data for all investigated particles

	Fresh	After reduction	Comment
F4S950	Fe_2O_3, SiO_2	–	
F4S1100	Fe_2O_3, SiO_2	–	
F4S1300	Fe_2O_3, SiO_2 (2)	–	
F4Z950	Fe_2O_3, ZrO_2	Fe_3O_4, ZrO_2	
F4Z1100	Fe_2O_3, ZrO_2	Fe_3O_4, ZrO_2	
F4Z1300	Fe_2O_3, ZrO_2, $ZrSiO_4$	Fe_3O_4, ZrO_2, $ZrSiO_4$	
F6AB1100	Fe_2O_3, Al_2O_3 (2)	Fe_2O_3, Fe_3O_4, Al_2O_3	
F6AB1200	Fe_2O_3, Al_2O_3 (2)	Fe_3O_4, Al_2O_3	
F6AB1300	Fe_2O_3, Al_2O_3 (2)	Fe_3O_4, Al_2O_3	
F4AM1100	Fe_2O_3, $Mg(Al,Fe)_2O_4$	$Mg(Al,Fe)_2O_4$	Uncertain
F4AM1200	$Mg(Al,Fe)_2O_4$	$Mg(Al,Fe)_2O_4$	Uncertain
F4AM1300	$Mg(Al,Fe)_2O_4$	$Mg(Al,Fe)_2O_4$	Uncertain
F6AM1100	Fe_2O_3, $Mg(Al,Fe)_2O_4$	$MgFeAlO_4$, $Mg(Al,Fe)_2O_4$	Uncertain
F6AM1125	Fe_2O_3, $Mg(Al,Fe)_2O_4$	$MgFeAlO_4$, $Mg(Al,Fe)_2O_4$	Uncertain
F6AM1150	Fe_2O_3, $Mg(Al,Fe)_2O_4$	$MgFeAlO_4$, $Mg(Al,Fe)_2O_4$	Uncertain
F6AM1175	Fe_2O_3, $Mg(Al,Fe)_2O_4$	$MgFeAlO_4$, $Mg(Al,Fe)_2O_4$	Uncertain
F6AM1200	Fe_2O_3, $Mg(Al,Fe)_2O_4$	$MgFeAlO_4$, $Mg(Al,Fe)_2O_4$	Uncertain
F8AM1100	Fe_2O_3, $Mg(Al,Fe)_2O_4$	$MgFe_3O_4$, $MgFeAlO_4$	Uncertain
F8AM1200	Fe_2O_3, $Mg(Al,Fe)_2O_4$	$MgFe_3O_4$, $MgFeAlO_4$	Uncertain
F8AM1300	Fe_2O_3, $Mg(Al,Fe)_2O_4$	$MgFe_3O_4$, $MgFeAlO_4$	Uncertain
M37S950	Mn_7SiO_{12}, SiO_2	–	Uncertain
M37S1100	Mn_7SiO_{12}, SiO_2 *etc*.	Mn_2SiO_4, SiO_2 *etc*.	Uncertain
M37S1200	$MnSiO_3$, SiO_2 (3)	$MnSiO_3$, SiO_2 (3)	Uncertain
M37S1300	Mn_7SiO_{12}, $MnSiO_3$, SiO_2 *etc*.	Mn_2SiO_4, $MnSiO_3$, SiO_2 *etc*.	Uncertain
M37Z950	Mn_3O_4, ZrO_2, C	MnO, ZrO_2	
M37Z1100	Mn_3O_4, ZrO_2, C	MnO, ZrO_2	
M37Z1300	Mn_3O_4, ZrO_2 (2)	MnO, ZrO_2 (2)	
M4CZ950	Mn_3O_4, ZrO_2, $Ca_{0.15}Zr_{0.85}O_{1.85}$	MnO, ZrO_2, $Ca_{0.15}Zr_{0.85}O_{1.85}$	
M4CZ1100	Mn_3O_4, ZrO_2, $Ca_{0.15}Zr_{0.85}O_{1.85}$	MnO, ZrO_2, $Ca_{0.15}Zr_{0.85}O_{1.85}$	
M4CZ1200	Mn_3O_4, ZrO_2, $Ca_{0.15}Zr_{0.85}O_{1.85}$	MnO, ZrO_2, $Ca_{0.15}Zr_{0.85}O_{1.85}$	
M4CZ1300	Mn_3O_4, ZrO_2	MnO, ZrO_2	
M4MZ950	Mn_3O_4, ZrO_2	MnO, ZrO_2	
M4MZ1100	Mn_3O_4, ZrO_2	MnO, ZrO_2	

Table 2. *Continuation*

	Fresh	After reduction	Comment
M4MZ1150	Mn_3O_4, ZrO_2	MnO, ZrO_2	
M4MZ1200	Mn_3O_4, ZrO_2	MnO, ZrO_2	
M4MZ1300	Mn_3O_4, ZrO_2	MnO, ZrO_2	
M4CeZ950	Mn_3O_4, ZrO_2, $Zr_{0.84}Ce_{0.16}O_2$	MnO, ZrO_2, $Zr_{0.84}Ce_{0.16}O_2$	
M4CeZ1100	Mn_3O_4, ZrO_2, $Zr_{0.84}Ce_{0.16}O_2$	MnO, ZrO_2, $Zr_{0.84}Ce_{0.16}O_2$	
M4CeZ1300	Mn_3O_4, ZrO_2, $Zr_{0.84}Ce_{0.16}O_2$	MnO, ZrO_2, $Zr_{0.84}Ce_{0.16}O_2$	
N4AN1300	NiO, $NiAl_2O_4$	Ni, $NiAl_2O_4$	
N4AN1600	NiO, $NiAl_2O_4$	Ni, $NiAl_2O_4$	
N4AC1400	NiO, $NiAl_2O_4$, $CaSiO_3$	Ni, $NiAl_2O_4$, $CaSiO_3$	
N4AC1600	–	–	
N4AB1300	NiO, $NiAl_2O_4$	Ni, $NiAl_2O_4$	
N6AM1400	NiO, $MgAl_2O_4$, $NiAl_2O_4$	Ni, $MgAl_2O_4$, $NiAl_2O_4$	
N6AM1500	NiO, $MgAl_2O_4$, $NiAl_2O_4$	Ni, $MgAl_2O_4$, $NiAl_2O_4$	
N6AM1600	NiO, $MgAl_2O_4$, $NiAl_2O_4$	Ni, $MgAl_2O_4$, $NiAl_2O_4$	
N6M1100	$MgNiO_2$	–	
N6M1200	$MgNiO_2$	–	
N6M1300	$MgNiO_2$	$MgNiO_2$	

Numbers in brackets indicate more than one type of phase

M37S1300, and N6M1300) there was formation of new compounds from sintering in the preparation process. There is an uncertainty regarding the suggested compounds from the XRD investigation on the M37S particles, as these are very hard to determine. However, it is clear that formation of manganese silicates has occurred. For all particles of Fe_2O_3 on $MgAl_2O_4$ the formation of new compounds from sintering also occurred. As with M37S, conclusive judgments about the solid phases were not possible from XRD. However in this case some of these phases are reducible in methane and therefore participate in subsequent oxygen removal and uptake during chemical-looping combustion. This has already been discussed by Johansson *et al*. [10]. ZrO_2 is the inert material that is least apt to form compounds with the metal oxides.

Conclusions

Chemical-looping combustion is a combustion technology with inherent separation of the greenhouse gas CO_2. The method uses an oxygen carrier to transport oxygen

from the air to the fuel. Results from reactivity, chemical composition and crushing strength tests of fifty oxygen carriers based on iron-, manganese-, and nickel oxides on different inert materials are presented. Reactivity tests under alternating oxidizing and reducing conditions were performed in a laboratory fluidized bed-reactor of quartz. Reduction was performed in 50% CH_4/50% H_2O while the oxidation was carried out in 5% O_2 in nitrogen. In general nickel particles are the most reactive, followed by manganese. Iron particles are harder but have a lower reactivity. An increase in sintering temperatures normally leads to an increase in strength and decrease in reactivity. Several particles investigated display a combination of high reactivity and strength as well as good fluidization behavior, and are feasible for use as oxygen carriers in chemical-looping combustion.

Acknowledgments

This work was financed by the ECSC project, Capture of CO_2 in Coal Combustion (CCCC), 7220-PR-125 and Swedish Energy Agency, project 20274-1.

References

[1] Anheden, M., Svedberg, G., Exergy Analysis of Chemical-Looping Combustion Systems *Energy Conversion and Management, 39* (1998), 16-18, pp. 1967-1980
[2] Ishida, M., Zheng, D., Akehata, T., Evaluation of a Chemical-Looping Combustion Power-Generation System by Graphic Exergy Analysis, *Energy, 12* (1987), 2, pp. 147-154
[3] Lyngfelt, A., Leckner, B., Mattisson, T., A Fluidized-Bed Combustion Process with Inherent CO_2 Separation; Application of Chemical-Looping Combustion, *Chemical Engineering Science, 56* (2001), 10, pp. 3101-3113
[4] Lyngfelt, A., Leckner, B., Technologies for CO_2 Separation, Minisymposium on Carbon Dioxide Capture and Storage, Chalmers University of Technology and Göteborg University, Göteborg, Sweden, 1999, available at www.entek.chalmers.se/~anly/
[5] Mattisson, T., Lyngfelt, A., Capture of CO_2 Using Chemical-Looping Combustion, in: Scandinavian-Nordic Section of Combustion Institute, Göteborg, Sweden, 2001, available at www.entek.chalmers.se/~anly/
[6] Cho, P., Mattisson, T., Lyngfelt, A., Carbon Formation on Nickel and Iron Oxide-Containing Oxygen Carriers for Chemical-Looping Combustion, *Industrial and Energy Chemistry Research, 44* (2005), 4, pp. 668-676
[7] Mattisson, T., Johansson, M., Lyngfelt, A., Multi-Cycle Reduction and Oxidation of Different Types of Iron Oxide Particles – Application of Chemical-Looping Combustion, *Energy & Fuels, 18* (2004), 3, pp. 628-637
[8] Adánez, J., de Diego, L. F., García-Labiano, F., Gayán, P., Abad, A., Palacios, J. M., Selection of Oxygen Carriers for Chemical-Looping Combustion, *Energy & Fuels, 18* (2004), 3, pp. 371-377
[9] Mattisson, T., *et al*., Capture of CO_2 in Coal Combustion (CCCC), ECSC Coal RTD programme, Final report, Project 7220-PR-125, 2005
[10] Johansson, M., Mattisson, T., Lyngfelt, A., Investigation of Fe_2O_3 with $MgAl_2O_4$ for Chemical-Looping Combustion, *Industrial and Energy Chemistry Research, 43* (2004), 22, pp. 6978-6987

[11] Cho, P., Mattisson, T., Lyngfelt, A., Defluidization Conditions for Fluidized-Bed of Iron, Nickel, and Manganese Oxide-Containing Oxygen-Carriers for Chemical-Looping Combustion, *Industrial and Engineering Chemistry Research, 45* (2006), 3, pp. 968-977
[12] Johansson, M., Mattisson, T., Lyngfelt, A., Investigation of Mn_3O_4 with Stabilized ZrO_2 for Chemical-Looping Combustion, *Chemical Engineering Research and Design, 84* (2006), 9A, pp. 795-806
[13] Abad, A., Mattisson, T., Lyngfelt, A., Rydén, M., Chemical-Looping Combustion in a 300 W Continuously Operating Reactor System Using a Manganese-Based Oxygen Carrier, *Fuel, 85* (2006), 9, pp. 1174-1185

Authors' addresses:

M. Johansson
Department of Chemical and Biological Engineering,
Division of Environmental Inorganic Chemistry
Chalmers University of Technology, S-412 96 Göteborg, Sweden

T. Mattisson, A. Lyngfelt
Department of Energy and Environment, Division of Energy Technology
Chalmers University of Technology, S-412 96 Göteborg, Sweden

Corresponding author (M. Johansson):
E-mail: marcus.johansson@chem.chalmers.se

Paper submitted: August 29, 2005
Paper revised: January 19, 2006
Paper accepted: March 14, 2006